

Magnetic structure near (310) tilt boundaries in iron

K. Hampel and D. D. Vvedensky

The Blakett Laboratory, Imperial College, London SW7 2BZ, United Kingdom

S. Crampin

Institute for Theoretical Physics, Catholic University of Nijmegen, Toernooiveld, NL-6525 ED Nijmegen, The Netherlands

(Received 4 December 1992)

The layer Korringa-Kohn-Rostoker method has been used to investigate the electronic and magnetic structure of an isolated, symmetric $\Sigma 5$ Fe (310) tilt boundary. The calculation shows an enhancement of the local magnetic moment at the grain boundary, which decays away rapidly from the region of the interface. The magnitude and form of the enhancement is similar to that found near iron surfaces from recent tight-binding calculations.

The interplay between magnetism and structure is an intriguing feature of iron and many studies have been devoted to studying various aspects of iron magnetism in different structural settings. The variety of magnetic structures shown by thin iron films grown on copper¹ surfaces attests to the richness of the magnetism-structure relationship. Iron is also an important technological material in its own right, and the quest for alloys of iron with ever more demanding mechanical, electrical, and magnetic properties remains a challenging area of research. For example, a ductile iron aluminide has been developed recently with properties that compete very well with stainless steel and other iron alloys.² This material combines high strength with good ductility, and appears to be more resistant to sulfidation than other alloys. At the same time, the cost of the material is relatively low.

Despite the considerable effort that has been invested in the study of magnetic surfaces and overlayers,¹ comparatively little is understood about the magnetic and electronic properties of grain boundaries. Much of the theoretical work on grain boundaries has involved using atomistic simulations to characterize the structure of the grain boundary and calculate the interface energy, or to compare the structure with x-ray measurements³ or high-resolution electron micrographs.⁴ Other approaches have used topological structural-unit models to describe the different types of structures that are possible at a grain boundary.^{5,6} The embedded-atom method has been used to model crack formation near Ni and Ni₃Al grain boundaries,⁷ and the applicability of the method to body-centered-cubic materials has been addressed recently.⁸ However, the magnetism of iron is certainly an inhibiting factor to applying the embedded-atom method because of the additional complications involved in determining the embedding function.

From the point of view of conventional *ab initio* electronic structure methods, grain boundaries present a formidable challenge because of the absence of translational symmetry. The use of a periodic array of grain boundaries might be contemplated, though even treating the simplest grain boundaries would require a large number

of unique atoms because of the small interlayer spacing. For the (310) grain boundary considered here, the interlayer spacing is $a/\sqrt{10}$, where a is the lattice constant. First-principles calculations have included tight-binding cluster calculations, which suffer from the drawback of including free interfaces, and so far fail to treat longer-range effects of d electrons. In addition, the extension of cluster methods to large systems is proving to be a formidable task particularly with regard to the embedding to remove the free boundaries. Semiconductor grain boundaries have been studied using tight-binding methods,⁹ and pseudopotential-simulated annealing techniques.¹⁰

In this paper we present results of a calculation on an isolated $\Sigma 5$ Fe (310) tilt boundary using the layer Korringa-Kohn-Rostoker¹¹ (LKRR) technique optimized for closely spaced layers.¹² In the LKRR method, the central quantity is the Green's function, $G(\mathbf{r}, \mathbf{r}; E, \sigma)$ at energy E and spin σ , which is calculated using multiple scattering theory. Once the Green's function has been obtained, other properties such as the density of states, charge density, and total energy may be derived. For example, the local charge density is given by $\rho(\mathbf{r}; E, \sigma) = -\pi^{-1} \text{Im}G(\mathbf{r}, \mathbf{r}; E, \sigma)$. The featureless structure of the Green's function even for moderate imaginary parts of the energy also has the added benefit of requiring fewer sampling points than for corresponding calculations on the real axis. The LKRR technique has already been applied to the calculation of stacking-fault energies in close-packed metals¹³ and has also been used to study an idealized tilt boundary in nickel.¹⁴

The LKRR Green's function is constructed by subdividing the system into layers, which may either be stacked periodically to recover three-dimensional translational symmetry, or embedded in a semi-infinite half-space of layers; the atoms comprising each layer need not be coplanar. The atomic potentials are constructed using the "muffin-tin" approximation. The scattering matrices of each atom are calculated in an angular momentum basis, from which the scattering matrices of each layer are calculated and expressed in a plane-wave basis. The layer-scattering matrices are used to construct the

scattering matrices of a sequence of layers or to embed a layer into an otherwise perfect solid by using layer composition and doubling algorithms.^{11,15} The stacking process has a natural cutoff with distance due to attenuation caused by the imaginary component in the energy, which means that a half-space may be constructed using very few iterations (typically less than 10) of the layer-doubling algorithm, corresponding to approximately 1000 layers.

The calculations of the iron grain boundary have been performed using an extension of the LKKR method for close-spaced layers (CSLKKR), which was chosen for its superior performance when treating high-Miller-index planes. If the interplanar spacing is small or the layer unit cell is very large then the number of plane waves required by conventional LKKR increases rapidly. This may be seen by looking at the form of the plane-wave basis functions which couple two adjacent layers: $\langle \mathbf{r} | \mathbf{K}_g^\pm \rangle = e^{i\mathbf{K}_g^\pm \cdot \mathbf{r}}$ where $\mathbf{K}_g^\pm = \mathbf{k} + \mathbf{g} + \hat{z}\sqrt{2E - |\mathbf{k} + \mathbf{g}|^2}$, \mathbf{g} is the two-dimensional reciprocal lattice vector, and \mathbf{k} is the two-dimensional crystalline momentum. As $g (=|\mathbf{g}|)$ increases, this basis function reduces to $\langle \mathbf{r} | \mathbf{K}_g^\pm \rangle = e^{i(\mathbf{k} + \mathbf{g}) \cdot \mathbf{c}_\parallel} e^{-g|c_z|}$, where the layers are separated by a vector $\mathbf{c} = (c_\parallel, c_z)$ and additional terms are attenuated by the increasing imaginary component of the momentum. This truncation of the basis set is less effective as the interlayer separation decreases for two reasons. First, as $|c|$ decreases the attenuation of each \mathbf{g} component decreases, and so makes a greater contribution to the expansion. Second, a reduction in the interlayer separation is usually accompanied by an increase in the layer unit cell vectors (volume per atom being approximately constant). Hence, the reciprocal lattice vectors \mathbf{g} comprise a more "compact" set of vectors, with more vectors shorter than a given length. Thus more vectors are needed, with the number rapidly increasing as the number of vectors of length g is proportional to g . This convergence problem is made more manageable in the CSLKKR technique by treating scattering from adjacent layers using an angular momentum basis set and further layers using a plane-wave basis.¹² The balancing of basis-set sizes reduces the size of the plane-wave basis quite considerably, allowing a significant reduction in the amount of computation required.

The calculations were performed with a basis of 25 plane waves and a spherical-wave basis up to $l=2$. The energy integral was performed using a triangular contour in the complex plane along which 32 sampling points were taken. The two-dimensional Brillouin-zone average was performed by taking sixteen special \mathbf{k} points using Cunningham's algorithm.¹⁶ The potentials for up to eleven layers on each side of the interface were allowed to relax self-consistently and the bulk potentials were calculated self-consistently using the same code and the same parameters as used for the interface calculation. The von Barth-Hedin form of the local-density functional¹⁷ was used.

The $\Sigma 5$ tilt boundary in a body-centered-cubic (bcc) structure is shown in Fig. 1. The structure has been relaxed to preserve nearest-neighbor distances by shifting the layers adjacent to the interface away from each other.

There is little evidence of lateral reconstruction in a surface determination for Fe (310) (Ref. 18) so we have assumed that any lateral displacement of the layers around the defect can be neglected.

The muffin-tin magnetic moment was calculated around each of the relaxed potentials from the spin-resolved muffin-tin charge densities and is displayed in Fig. 2 along with the bulk values calculated for the moment. The enhancement of the magnetic moment is limited to the two layers adjacent to the interface, but there remains a small fluctuation in the moment further away from the defect which rapidly decays to the bulk value. This behavior is similar to a related calculation of an Fe $\Sigma 3$ tilt boundary.¹⁹ The enhancement is thought to be due largely to the increased volume around the defect layer along with reduced coordination of nearest and second-nearest neighbors. The magnitude of the moment enhancement and the profile of the relaxation away from the grain boundary is qualitatively similar to those calcu-

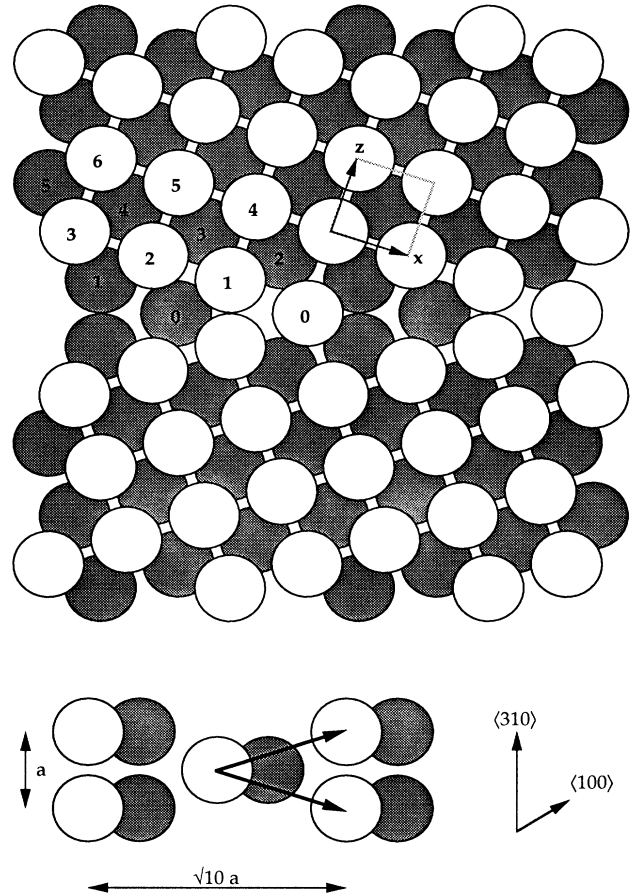


FIG. 1. The structure of an Fe (310) tilt boundary as used in the calculation. The layers are numbered starting with layer 0 at the interface. The shaded circles represent atoms further into the page. Note the increased interplanar spacing around the interface layer, which has been introduced to prevent overlap of muffin tins. The shaded box indicates the conventional bcc unit cell, with the unit z axis and x axis labeled. Also shown is the interface layer (0) and one of the nearest layers (1) in the (310) direction.

lated for iron surfaces,^{20,21} as shown in Fig. 2 for a (100) surface.

Before examining the details of the contributions to the moments of each layer, we make some general observations concerning the basis functions of the irreducible representations along the principal directions in k space for the band structure of iron. In bulk crystalline iron, the five d orbitals transform as a two-dimensional and as a three-dimensional irreducible representation of the octahedral point group: $e_g = (d_{z^2}, d_{x^2-y^2})$ and $t_{2g} = (d_{xy}, d_{yz}, d_{xz})$. Of these, only the t_{2g} levels contribute to broad Λ_1 bands along the nearest-neighbor direction, while both the e_g and t_{2g} levels contribute to the narrower Λ_3 bands. Only the d_{z^2} level contributes to the broad Δ_1 and Σ_1 bands along the (100) and (110) directions, respectively, while the $d_{x^2-y^2}$ level contributes to the comparatively narrow Δ_2 and Σ_4 bands. We therefore expect that the d_{xy} , d_{xz} , and d_{yz} , and d_{x^2} levels are the most strongly perturbed by the presence of the grain boundary, with the $d_{x^2-y^2}$ levels showing a much weaker susceptibility.

A symmetry-resolved breakdown of the contribution to the muffin-tin magnetic moment of the d electrons is shown in Fig. 3. The d orbitals have been expressed in the coordinate system of the conventional bcc unit cell, with the axes as shown in Fig. 1. The values shown for layer 12 are taken from a separate calculation of the perfect crystalline system. The absence of degeneracy in the

two sets of orbitals away from the interface is an artifact of the calculation. If the plane-wave basis set was infinite and the Brillouin-zone integration was continuous, then degeneracy would be restored far from the grain boundary. However, the error is not large enough to mask gross trends in the behavior of the local moment. The graph shows that, to a good approximation, bulklike behavior is obtained beyond layer 4. This indicates that a majority of the enhanced moment is due to perturbations in the nearest-neighbor environment.

The behavior of the magnetic moment of the d_{z^2} orbitals may be readily explained. There is increased separation between d_{z^2} orbitals in the z direction in the grain-boundary layer and to a lesser extent for layers 2 and 3. However, there is greater overlap between the orbitals in layer 1, due to the symmetrical stacking of the fault, which increases the overlap among neighboring orbitals. This corresponds directly with the behavior of the moment.

The contribution to the moment from the $d_{x^2-y^2}$ orbital is comparatively unaffected, but exhibits the same general trend as that of the d_{z^2} ; on the other hand, the d_{xy} orbital contributes strongly to the moment enhancement. These trends again may be explained from the directions of the orbitals in relation to changes to nearest- and second-nearest-neighbor environment. The lobes of the $d_{x^2-y^2}$ orbital point along the coordinate axes (toward the second-nearest neighbors), so a majority of the lobes

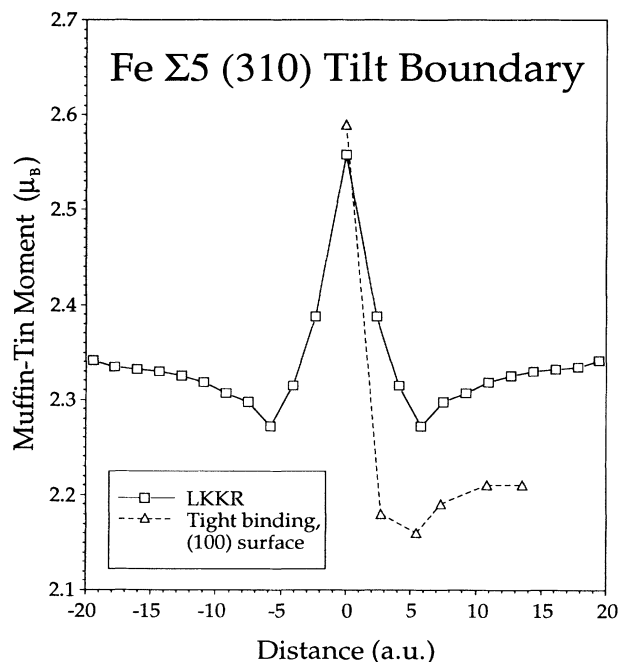


FIG. 2. A layer-by-layer breakdown of the local magnetic muffin-tin moment around the Σ_5 tilt boundary. The potentials of 10 layers each side of the boundary are allowed to relax, the eleventh layer has a frozen bulk potential. Also shown for comparison is an 11-layer (100) surface calculation, which was obtained using a tight-binding cluster calculation (Ref. 21).

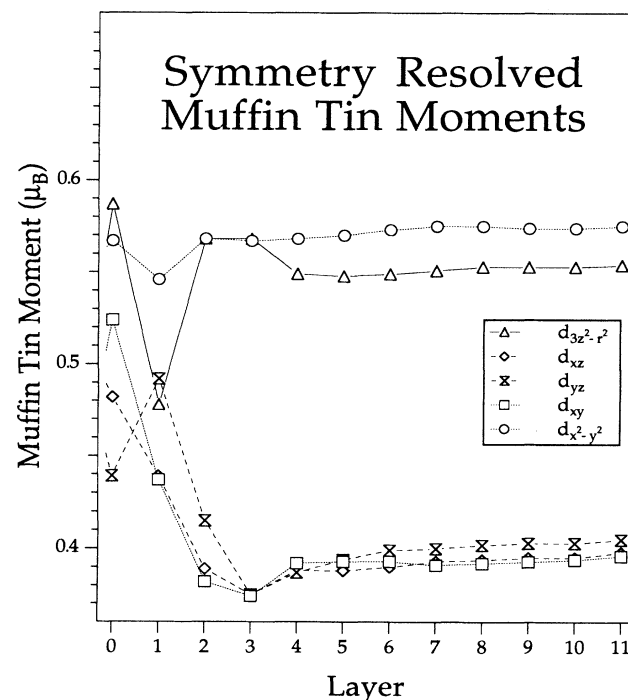


FIG. 3. A symmetry-resolved layer-by-layer breakdown of the contribution of d electrons to the local muffin-tin moment. The z axis is the normal to the plane of the defect (the $\langle 310 \rangle$ direction) and the x axis is the long side of the unit cell shown in Fig. 1.

of the orbital do not see any change in environment. The d_{xy} orbital is more susceptible both to the changes in volume and in the nearest-neighbor coordination number associated with the grain boundary, and is thus more severely perturbed. The d_{xz} and d_{yz} are less strongly affected, but still show a pronounced enhancement of the magnetic moment.

The gross trends found for the magnetic perturbations near Fe $\Sigma 3$ tilt boundaries are qualitatively similar to those found for the electronic perturbations near Ni $\Sigma 5$ tilt boundaries reported earlier.¹⁴ The changes near the boundary are driven by the changes in coordination number and coordination geometry, which inhibit bonding among the directional d orbitals which, in turn, results in narrower band widths. In the case of iron, the band narrowing promotes a strong enhancement of the magnetic moment. The "healing" of these electronic perturbations is complete by the fifth layer, beyond which essentially bulklike electronic structure is found.

The reduced bonding near the interface makes polycrystalline iron susceptible to nonmetallic impurities such as S, which tend to segregate to the grain boundaries and induce brittle fracture behavior. The calculations presented here can provide a test bed for the introduction

of segregated substitutional or interstitial impurities which could provide information useful in the determination of the magnetic properties of variously processed steels. However, properties such as the structure of the grain boundary, which require the calculation of the total energy are still beyond the currently available techniques. However, integration schemes for arbitrarily shaped Wigner-Seitz cells,²² leading to full potential versions of LKKR theory will make such calculations possible. Also, once more realistic structural relaxations are known, then these too may be fed into the calculation as an aid to discovering the overall picture of structure-magnetism-property relationships.

This work was supported by the Office of Naval Research and by the Nippon Steel Corporation and the Nissan Motor Company, Ltd. through the Consortium for Computationally-Assisted Materials Development at Imperial College. S.C. would also like to acknowledge the support of the Royal Society. K.H. would also like to thank Professor David Pettifor for several helpful discussions and Dr. J. Takimoto of Nissan Central Engineering Laboratories, where some of the work was performed.

-
- ¹L. Falicov, D. Pierce, S. Bader, R. Gronsky, K. Hathaway, H. J. Hopster, D. Lambeth, S. Parkin, G. Printz, M. Salamon, I. Schuller, and R. Victoria, *J. Mater. Res.* **5**, 1299 (1990).
- ²MRS Bull. **XVI**, 9 (1991).
- ³M. R. Fitzsimmons and S. L. Sass, *Acta Metall.* **36**, 3103 (1988); **37**, 1009 (1989).
- ⁴U. Dahmen, C. J. D. Hetherington, M. A. O'Keefe, K. H. Westmacott, M. J. Mills, M. S. Daw, and V. Vitek, *Philos. Mag. Lett.* **62**, 327 (1990).
- ⁵M. F. Ashby, F. Spaepen, and S. Williams, *Acta Metall.* **26**, 1647 (1978).
- ⁶N. Rivier, in *Quasicrystals and Incommensurate Structures in Condensed Matter*, edited by M. I. Yacaman, D. Romeu, V. Castano, and A. Gomez (World Scientific, Singapore, 1990).
- ⁷M. I. Baskes, S. M. Foiles, and M. S. Daw, *J. Phys. (Paris) Colloq.* **C5-49**, 483 (1988); M. S. Daw, M. I. Baskes, and W. G. Wolfer, *Proceedings of the Special Symposium on Modelling Environmental Effects on Crack Initiation and Propagation* (AIME, New York, 1985).
- ⁸J. B. Adams and S. M. Foiles, *Phys. Rev. B* **41**, 3316 (1990).
- ⁹M. Kohyama, R. Yamamoto, Y. Ebata, and M. Kinoshita, *J. Phys. C* **21**, 3205 (1988).
- ¹⁰E. Tarnow, P. Dallot, P. D. Bristowe, J. D. Joannopoulos, G. P. Francis, and M. C. Payne, *Phys. Rev. B* **42**, 3644 (1990).
- ¹¹J. M. MacLaren, S. Crampin, D. D. Vvedensky, and J. B. Pendry, *Phys. Rev. B* **40**, 12 164 (1989); J. M. MacLaren, S. Crampin, D. D. Vvedensky, R. C. Albers, and J. B. Pendry, *Comput. Phys. Commun.* **60**, 365 (1990).
- ¹²J. M. MacLaren, S. Crampin, and D. D. Vvedensky, *Phys. Rev. B* **40**, 12 176 (1989).
- ¹³S. Crampin, K. Hampel, D. D. Vvedensky, and J. M. MacLaren, *J. Mater. Res.* **5**, 2107 (1990).
- ¹⁴S. Crampin, D. D. Vvedensky, J. M. MacLaren, and M. E. Eberhart, *Phys. Rev. B* **40**, 3413 (1989).
- ¹⁵J. B. Pendry, *Low Energy Electron Diffraction* (Academic, London, 1974).
- ¹⁶S. L. Cunningham, *Phys. Rev. B* **10**, 1988 (1974).
- ¹⁷U. von Barth and L. Hedin, *J. Phys. C* **5**, 1200 (1972).
- ¹⁸J. Sokolov, F. Jona, and P. M. Markus, *Phys. Rev. B* **29**, 5402 (1984).
- ¹⁹A. Gonis, X.-G. Zhang, J. M. MacLaren, and S. Crampin, *Phys. Rev. B* **42**, 3798 (1990).
- ²⁰S. Ohnishi, A. J. Freeman, and M. Weinert, *Phys. Rev. B* **28**, 6741 (1983).
- ²¹A. Mokrani, C. Demangeat, and H. Dreysse, *Phys. Rev. B* **42**, 8670 (1990).
- ²²N. Stefanou, H. Akai, and R. Zeller, *Comput. Phys. Commun.* **60**, 231 (1990).